Journal of The Electrochemical Society, **156** (9) F109-F114 (2009)
0013-4651/2009/156(9)/F109/6/$25.00 © The Electrochemical Society

Numerical Simulation of Ionic Mass-Transfer Rates with Natural Convection in $CuSO_4$–H_2SO_4 Solution

II. Comparisons Between Numerical Calculations and Optical Measurements

S. Kawai,[a] Y. Fukunaka,[b,*,z] and S. Kida[a]

[a]*Department of Mechanical Engineering and Science, Kyoto University, Kyoto 606-8501, Japan*
[b]*Nano Technology Research Center, Waseda University, Tokyo 162-0041, Japan*

A mathematical model is developed in Part I of this study for the ionic mass-transfer rates associated with natural convection developing along both electrodes immersed in a $CuSO_4$ aqueous electrolyte. The additional effect of an excess amount of H_2SO_4 is discussed through the comparisons with the optical measurements. The concentration profiles of both Cu^{2+} and H^+ ions and the natural convective velocity profile have been measured by a two-wavelength holographic interferometer and the tracer method. The present calculation quantitatively agrees with the measured ionic mass-transfer rates toward the electrode surface except for copper electrolysis in an unsupported $CuSO_4$ electrolyte above one-half of the limiting current density. The optical observation suggests that a substantially steady state is attained within 180 s after starting the electrolysis in every case. The numerical calculation predicts a further development of ionic mass-transfer phenomena over 600 s. It is closely related to both secondary flow and electrolyte stratification phenomena.
 [DOI: 10.1149/1.3158831]

Manuscript submitted September 24, 2008; revised manuscript received May 27, 2009. Published July 9, 2009.

The electrolytic refining and winning processes easily supply the high purity metals such as copper, silver, and zinc by applying the electric energy. However, the engineering problem about the limited productivity of electrolytic metals per unit area of a two-dimensional (2D) electrode surface must be overcome. It is well known that the current density distribution readily becomes nonuniform during a higher current density operation. The undesirable side reactions, such as dendritic or needlelike electrodeposited metal growth and gas evolution, are also induced.

Copper refining electrolysis is one of the most important industrial electrolytic processes, where 1 m high vertical plane electrode surfaces are placed face to face, separated by 3–5 cm thick electrolyte layers. The modernized copper refining process is operated at a relatively high current density of more than 250 A/m^2. Therefore, the predictions of both limiting current density and criterion of uniform current density distribution are indispensable. Numerical simulation is required to analyze the large-scale industrial electrochemical process, including the electrolyte circulation system in the electrolytic tankhouse.

Since Wagner's pioneering work,[1] numerous theoretical and experimental studies have been made on the current density distribution as well as on the ionic mass-transfer rate associated with natural convection along the vertical plane cathode[2-10] and anode[11-13] installed in an unstirred $CuSO_4$ or $CuSO_4$–H_2SO_4 aqueous electrolyte solution. Most studies have dealt only with steady state, while only a few studies have been made on the transient or unsteady-state phenomena under the limiting current condition.[14] Many theoretical and numerical studies have been reported on the current density distribution as well as on the ionic mass-transfer phenomena in various electrochemical systems such as the rotating disk electrode system[15-19] and the parallel or tubular electrode systems.[20-25] However, a few studies have been carried out on the current-density distribution in the vertical plane electrode system most popularly employed in the industrial electrolysis process such as copper electrorefining.[8,26,27]

The present study numerically calculates a mathematical model developed in Part I of this study. The calculated transient behavior of ionic mass-transfer rate is compared with the optical measurements[7,11] to focus on the effects of both secondary flow and electrolyte stratification phenomena.

* Electrochemical Society Active Member.
z E-mail: fukunaka@energy.kyoto-u.ac.jp

Experimental

The experimental apparatus and setup were mentioned in Part I. Both 16 cm high anode and cathode were vertically installed face to face in a cell, separated by a 4.8 cm thick electrolyte layer. Two electrolyte compositions were employed: 0.05 M $CuSO_4$ and 0.05 M $CuSO_4$–1.85 M H_2SO_4. A constant electrolytic current was applied to the cathode. The electrolytic conditions in the present study are listed in Table I.

The concentration profiles of both Cu^{2+} and H^+ ions and the velocity profile developed along the vertical plane electrode were in situ measured by the two-wavelength holographic interferometer and the tracer technique, respectively.[7,11,12] A holographic interferometer measures the refractive index profile of an electrolyte solution. The relationship between the refractive index and the concentrations of solute species must be known in advance to interpret the interference fringe shift. The dependences of the refractive index of an electrolyte solution on the electrolyte composition and concentration were measured by Abbe's refractometer, and the following regression equations for the concentration dependence of the refractive index of an electrolyte solution were obtained.

1. For a 0.05 M $CuSO_4$ aqueous electrolyte

$$\Delta n_I = 0.02944 \Delta C_1 \quad [1]$$

2. For a 0.05 M $CuSO_4$–1.85 M H_2SO_4 aqueous electrolyte

$$\Delta n_I = 0.023527 \Delta C_1 - 0.010118 \Delta C_2 \quad [2]$$

$$\Delta n_{II} = 0.023718 \Delta C_1 - 0.010912 \Delta C_2 \quad [3]$$

Here, subscripts I and II represent the light sources employed in the present experiment. A He–Ne laser of wavelength at 632.8 nm

Table I. Experimental conditions.

(A) Composition of electrolyte: 0.05 M $CuSO_4$	
Average current density i_{av} (mA/cm^2)	0.236, 0.473, 0.946, 1.42, 1.96, 3.65, 4.6
(B) Composition of electrolyte: 0.05 M $CuSO_4$–1.85 M H_2SO_4	
Average current density i_{av} (mA/cm^2)	0.236, 0.473, 0.946, 1.42, 1.96
Electrode spacing L (cm)	4.8
Temperature T (K)	293

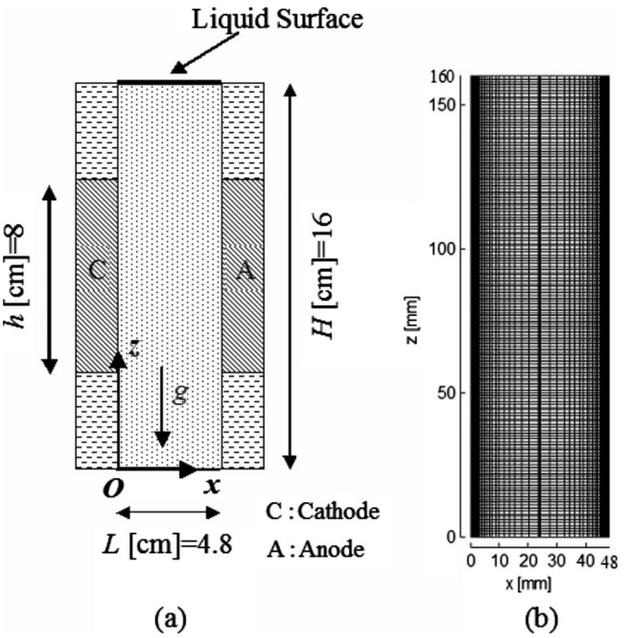

Figure 1. (a) Schematic diagram of 2D electrolytic cell and (b) unevenly divided grid used in numerical calculation.

and an Ar laser of wavelength at 457.9 nm were employed as the light sources.[7,11] Subscripts 1 and 2 express the ion species Cu^{2+} and H^+, respectively. The focal plane was fixed at the centerline of the effective electrode surface 5 mm wide. It was because the optical deflection effect in a steep refractive index gradient could be restricted to be as small as possible under such an optical arrangement. The measurement position of both concentration and velocity profiles was located at 4 cm from the lower edge of the effective electrode. The present measurement was mostly interrupted 300–600 s after starting the electrolysis.

Numerical Analysis

The mathematical model and the numerical calculation procedure have been described in Part I. It is based on several assumptions such as electroneutrality, acid–base equilibrium, Boussinesq approximation, and constant physical properties. Boundary condition modeling is based on the assumption that only the electrochemical deposition and dissolution of copper occur at the electrode/electrolyte interface and that no other reaction, such as gas evolution, takes place. A 2D mathematical model is numerically analyzed based on the marker-and-cell method using the finite difference method and the deterministic relaxation techniques.[28,29] Figure 1a shows the schematic diagram of the 2D electrolytic cell. The computational mesh of 120 × 160 cells employed in the numerical calculation is shown in Fig. 1b. The physical properties used in the present numerical calculation are listed in Table II.[6,11]

Results and Discussion

Transient variations in interference fringe pattern.— Figure 2 shows a typical example of the transient behavior of the interference fringe pattern in a 0.05 M $CuSO_4$ electrolyte at $i = 1.96$ mA/cm^2 considerably less than the limiting current density. The interference fringe pattern appears perpendicular to the cathode surface before electrolysis (a) and then shifts downward near the cathode surface with time after starting the electrolysis [(b) and (c)]. It seems to reach a substantially steady state at around 180 s.

The measured transient variation in refractive index profile in a 0.05 M $CuSO_4$–1.85 M H_2SO_4 electrolyte at the limiting current density of $i = 1.96$ mA/cm^2 is illustrated in Fig. 3. The interference fringe shift number no longer changes over 120 s. It may suggest that the limiting current condition is partially established over 120 s. The most different point from the numerical calculation is that the present optical measurement by the holographic interferometer could not detect the fluctuating behavior in the transient variations in electrode surface concentration, as seen in the calculated result (Fig. 8 in Part I of this study). The amplitude of such an oscillation can be estimated to be less than 5.0×10^{-4} M in the present numerical simulation. Such a very small concentration variation is within the measurement error of the present optical setup.

Table II. Physical constants.

(A) Composition of electrolyte: 0.05 M $CuSO_4$	
ν (m^2/s)	1.0×10^{-6}
D_A (m^2/s)	6.5×10^{-10}
α_A(m^3/mol)	1.6×10^{-4}
$^*t_1$	0.36
ρ_0 (kg/m^3)	0.99×10^3
σ (S/m)	0.5
(B) Composition of electrolyte:0.05 M $CuSO_4$–1.85 M H_2SO_4	
ν (m^2/s)	1.15×10^{-6}
D_A (m^2/s)	5.74×10^{-10}
α_A (m^3/mol)	1.25×10^{-4}
α_B (m^3/mol)	2.68×10^{-5}
$^*t_1$	0.0033
$^*t_2$	0.81
ρ_0 (kg/m^3)	1.12×10^3
σ (S/m)	51
a	0.31

Comparisons between calculations and measurements.— Figure 4 compares the transient variations in the measured cathode surface Cu^{2+} ion concentration at the middle of the effective electrode height with the present calculation at various current densities in 0.05 M $CuSO_4$. The dashed lines correspond to the analytical solutions for the unsteady one-dimensional diffusion equation in semi-infinite media, which can be expressed as follows

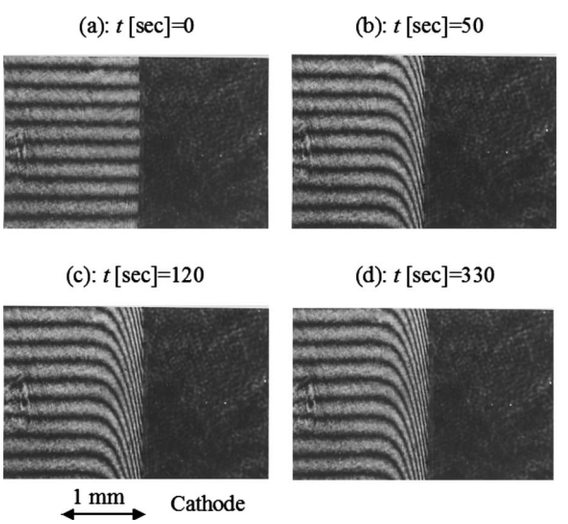

Figure 2. Holographic interferograms of cathodic diffusion layer at mid-height (0.05 M $CuSO_4$ solution, $i = 1.96$ mA/cm^2, and $^*z = 4$ cm). (a) $t = 0$ s, (b) $t = 50$ s, (c) $t = 120$ s, and (d) $t = 330$ s.

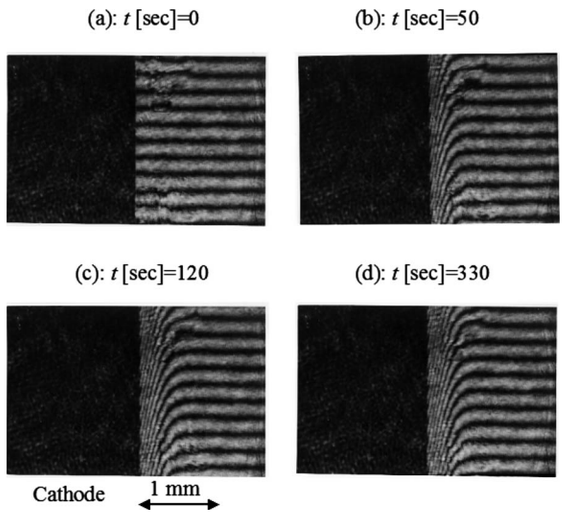

Figure 3. Holographic interferograms of cathodic diffusion layer at midheight (0.05 M $CuSO_4$–1.85 M H_2SO_4 solution, i = 1.96 mA/cm^2, and $^*z$ = 4 cm). (a) t = 0 s, (b) t = 50 s, (c) t = 120 s, and (d) t = 330 s.

$$C_{1,C}(t) = C_{1,0} + \frac{2(1.0 - {}^*t_1)i_{av}}{z_1 F}\sqrt{\frac{t}{\pi D_A}} \qquad [4]$$

Here, $^*t_1$ and z_1 express the transference number and the valency of the Cu^{2+} ion, respectively. F is the Faraday constant, t is the time, i_{av} is the applied average current density, and D_A expresses the diffusion coefficient of $CuSO_4$. $C_{1,C}$ and $C_{1,0}$ denote the cathode surface and bulk electrolyte concentrations of the Cu^{2+} ion, respectively. Calculated results are plotted at a 6 s interval. Calculated results quantitatively agree well with the analytical solutions, while the measured values are always higher than both analytical solutions and numerical calculations. The slopes estimated from the optical measurement in Fig. 4 are slightly smaller than those estimated from both numerical calculation and analytical solution. Such a deviation may be due to the less accuracy of the present method of focal plane in the optical arrangement because the accuracy of the present optical measurement strongly depends on the optical arrangement of the focal plane. Because the concentration difference between the electrode surface and the bulk electrolyte concentrations is proportional to this slope at the initial stage, the more apparent deviation is expected at the higher current density.

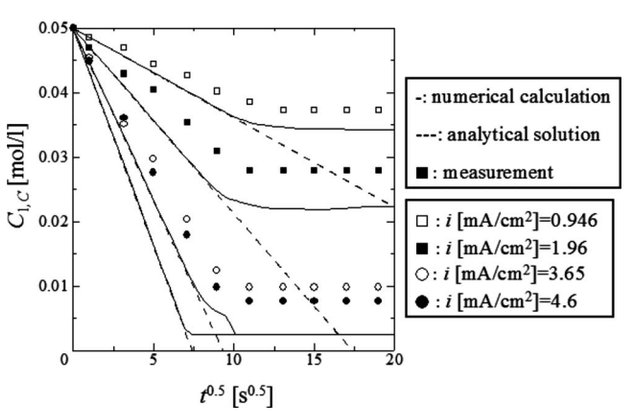

Figure 4. Transient variations in cathode-surface Cu^{2+} ion concentration at midheight (0.05 M $CuSO_4$ solution; $^*z$ = 4 cm). (-) Numerical calculation. (- - -) Analytical solution.

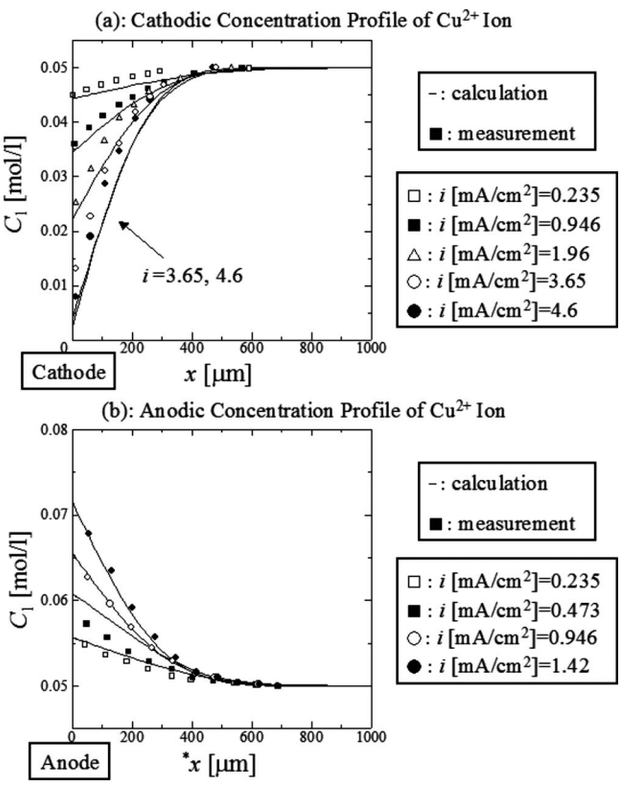

Figure 5. Concentration profiles of Cu^{2+} ion at midheight at 600 s after starting the electrolysis at various current densities (0.05 M $CuSO_4$ solution, $^*z$ = 4 cm, and t = 600 s). (a) Cathodic concentration profile of Cu^{2+} ion. (b) Anodic concentration profile of Cu^{2+} ion.

Both calculated and measured cathode surface Cu^{2+} ion concentrations initially decrease proportional to the square root of time, which implies that the ionic mass-transfer phenomena due to both diffusion and ionic migration effects are initially predominant. As natural convection develops along the vertical cathode with time, the electrode surface concentration then converges to a substantially steady-state value.

Figure 5 also compares the calculated concentration profile of the Cu^{2+} ion near the cathode surface with the measurement at 600 s after starting the electrolysis in a 0.05 M $CuSO_4$ electrolyte at various current densities. The present numerical calculation quantitatively predicts both cathodic and anodic concentration profiles of the Cu^{2+} ion below one-half of the limiting current density. However, a deviation between calculated and measured results becomes significant at i = 3.65 and 4.6 mA/cm^2, although the optical deflection effect is partly corrected.[6,7,30,31] It is deeply related to the above-mentioned present method of focal plane in the optical arrangement. Another reason may be referred to the assumption of constant physical properties, which may no longer be sound under the limiting current condition without a supporting electrolyte. The variations in transport properties with electrolyte concentration introduce a serious problem in numerical simulation at a high level current density.

The calculated concentration profiles of both Cu^{2+} and H^+ ions are compared with the measurements in a $CuSO_4$–H_2SO_4 electrolyte solution by the two-wavelength holographic interferometer at 600 s in Fig. 6 and 7, respectively. The quantitative agreements between both calculated and measured results are noticed in both cathodic and anodic concentration profiles of the Cu^{2+} ion. Moreover, in the concentration profile of the H^+ ion, both calculated and measured values quantitatively agree with each other near the electrode surface, while the calculated concentration boundary layer (CBL) thickness is apparently larger than the optically measured one. The

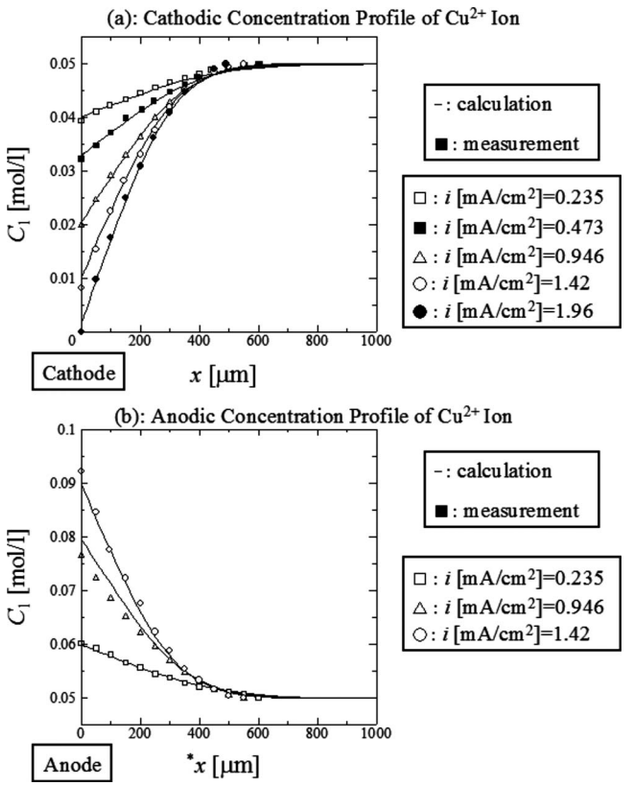

Figure 6. Concentration profiles of Cu^{2+} ion at midheight at 600 s after starting the electrolysis at various current densities (0.05 M $CuSO_4$–1.85 M H_2SO_4 solution, $^*z$ = 4 cm, and t = 600 s). (a) Cathodic concentration profile of Cu^{2+} ion. (b) Anodic concentration profile of Cu^{2+} ion.

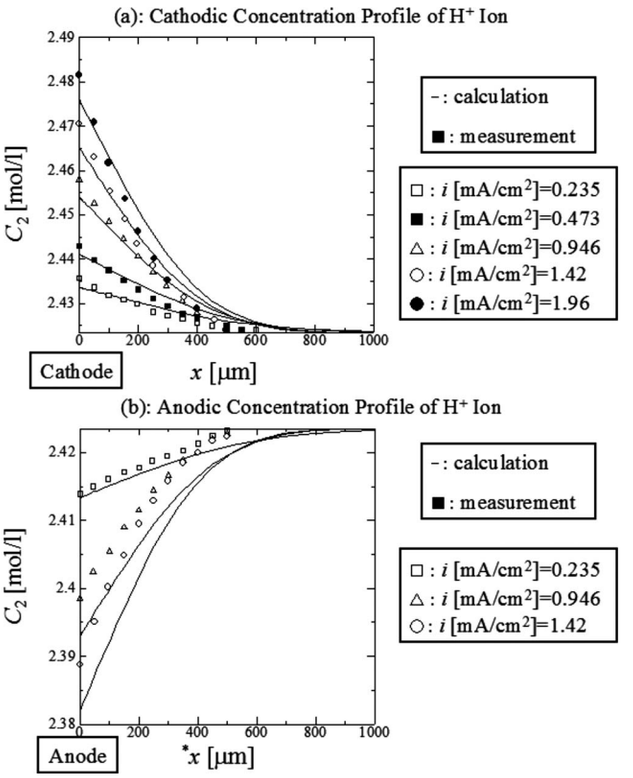

Figure 7. Concentration profiles of H^+ ion at midheight at 600 s after starting the electrolysis at various current densities (0.05 M $CuSO_4$–1.85 M H_2SO_4 solution, $^*z$ = 4 cm, and t = 600 s). (a) Cathodic concentration profile of H^+ ion. (b) Anodic concentration profile of H^+ ion.

CBL thickness for the H^+ ion is about 1.4 times larger than that for the Cu^{2+} ion in the present calculation. Surprisingly, the calculated electrode surface concentrations of both Cu^{2+} and H^+ ions agree well with the optical measurements even at the limiting current density. It may be because the boundary condition modeling for the H^+ ion is valid to some extent because H^+ ion concentration changes only within 5% of the bulk concentration.

The cathodic upward natural convective velocity profile is also compared in Fig. 8. The numerical calculation predicts a velocity profile similar to the measurement by the tracer method near the cathode surface, while a deviation between the calculated and measured results becomes significant in the region of the bulk electrolyte. A similar deviation in the bulk electrolyte region has been reported previously for an unsupported 0.6 M $CuSO_4$ electrolyte in the same electrolytic cell.[27] It must be caused by the experimental difficulty to make an electrolyte solution perfectly settled down in a stagnant condition.

Adding effect of an excess amount of H_2SO_4 on natural convection.— Copper electrolysis has been carried out galvanostatically at i = 1.96 mA/cm^2 in both electrolyte compositions of 0.05 M $CuSO_4$ and 0.05 M $CuSO_4$–1.85 M H_2SO_4. Figure 9 shows the cathodic concentration profile of the Cu^{2+} ion (a) and the cathodic natural convective velocity profile (b) in two electrolyte compositions. The Cu^{2+} ion concentration gradient toward the cathode surface in a $CuSO_4$–H_2SO_4 electrolyte is apparently steeper because the transference number of the Cu^{2+} ion is remarkably small due to the higher mobility of the H^+ ion. As clearly seen in Fig. 9b, both numerical calculation and experimental measurement show the damping effect caused by the addition of an excess amount of H_2SO_4 as a supporting electrolyte. In a 0.05 M $CuSO_4$, the maximal natural convective velocity in the present measurement is a little larger than that in the numerical calculation. Such a difference may be caused by the overshoot or oscillation behavior in the maximal velocity. As shown in the calculated results (Fig. 9 in Part I of this study), such a velocity oscillation is of the order of 0.05 mm/s, which is within the measurement error of the present tracer technique. The more accurate measurement method and procedure are necessary to examine both the oscillating behavior that appeared in the maximal natural convective velocity and the small but not negligible motion in the region of the bulk electrolyte.

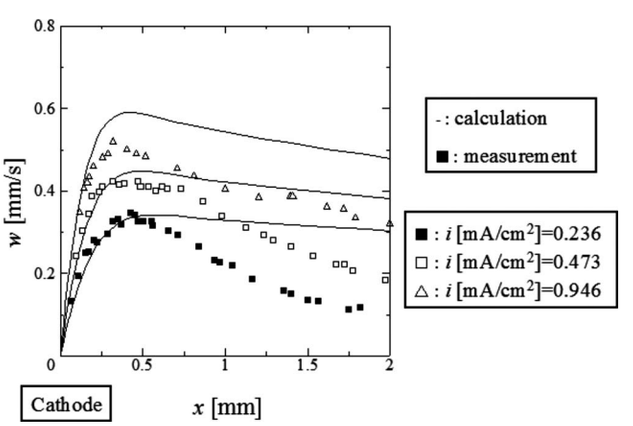

Figure 8. Cathodic natural convective velocity profiles at midheight at 600 s after starting the electrolysis at various current densities (0.05 M $CuSO_4$–1.85 M H_2SO_4 solution, $^*z$ = 4 cm, and t = 600 s).

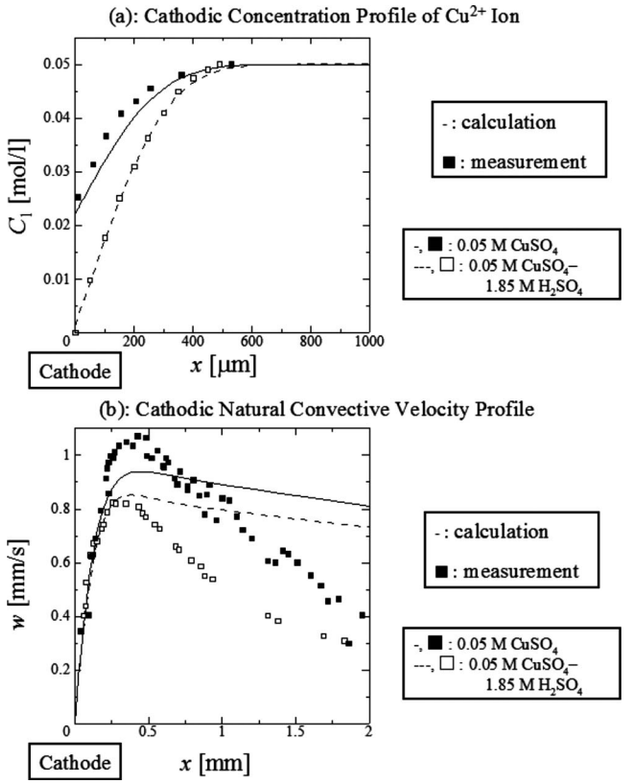

Figure 9. Comparison between two electrolyte compositions at midheight at 600 s after starting the electrolysis at the same current density (i = 1.946 mA/cm^2, $^*z$ = 4 cm, and t = 600 s). (a) Cathodic concentration profile of Cu^{2+} ion. (b) Cathodic natural convective velocity profile.

Conclusion

The mathematical model developed in Part I of this study is numerically calculated, and calculated results are compared with optical measurements by the holographic interferometry and the tracer method. Based on both our present and previous studies, a brief summary of the discussion about the transient ionic mass-transfer phenomena associated with natural convection in a high Schmidt number is given as follows.

1. The transient behaviors of the electrode surface ion concentration can be divided into three regions.

(A) The ionic mass-transfer phenomena due to both diffusion and ionic migration effects are initially predominant.

(B) Natural convection develops with time along the working electrode surface, and the electrode surface concentration gradually converges to a substantially steady-state value.

(C) At a certain time after starting the electrolysis, natural convection along the working electrode surface starts to interfere with that along the counter electrode surface. Small vortices appearing near both upper and lower edges of the effective electrodes significantly distort the electrolyte flow pattern in the region of the bulk electrolyte sandwiched by two vertical plane electrodes, which results in the periodic fluctuating electrolyte flow phenomena.

2. The magnitudes of the ionic mass-transfer rates by (B) and (C) are deeply related to the cell dimensions such as the electrode height, the interelectrode distance, the electrode configuration, and the magnitude of applied current density.

3. The deceleration in natural convective velocity can be detected in the present calculation at a high level current density, which is a very important phenomenon associated with electrolyte stratification that appeared at a longer period of duration time. Further experimental and numerical studies on the effects of both secondary flow and electrolyte stratification phenomena are indispensable because the conventional electrorefining cell is operated for several weeks.

4. The transient variations in maximal natural convective velocity take much more time to approach a substantially steady state than the transient variations in electrode surface ion concentration. It is closely related to the Schmidt number. Because the CBL thickness is much thinner than the hydrodynamic boundary layer thickness in the high Schmidt number case, the effect of the secondary flow velocity changes in the transient convective mass transfer is far less significant than that in the low Schmidt number. Hence, the concentration fluctuation in the CBL is damped out more rapidly than the velocity fluctuation in the hydrodynamic boundary layer.

Waseda University assisted in meeting the publication costs of this article.

List of Symbols

a	degree of dissociation of the HSO_4^- ion
C_i	concentration of ion species i, mol m^{-3}
$C_{i,0}$	concentration of ion species i in bulk electrolyte, mol m^{-3}
$C_{i,C}$	concentration of an ion species i at the cathode surface, mol m^{-3}
D_i	diffusion coefficient of an ion species or electroneutral compound i, m^2 s^{-1}
F	Faraday's constant/96,500 C/equiv
h	height of the effective electrode, m
H	height of an electrolyte free surface from the bottom of a cell, m
i	current density, A m^{-2}
i_{av}	average current density, A m^{-2}
L	interelectrode spacing, m
n_i	refractive index
Δn_i	refractive index difference from bulk the electrolyte
t	time, s
$^*t_i$	transference number of ion species i
T	temperature, K
w	vertical component of the fluid velocity of an electrolyte, m s^{-1}
x	horizontal distance from the cathode surface, m
$^*x$	horizontal distance from the anode surface, m
z	vertical distance from the bottom of a cell, m
$^*z$	vertical distance from the lower edge of effective electrode, m
z_i	valency of ion species i, g eq mol^{-1}

Greek

α_i	densification coefficient of an electroneutral compound i, m^3 mol^{-1}
λ	wavelength, m
ν	kinematic viscosity of an electrolyte, m^2 s^{-1}
ρ	fluid density of an electrolyte, kg m^{-3}
ρ_0	fluid density of bulk an electrolyte, kg m^{-3}
σ	electric conductivity of an electrolyte, S m^{-1}

Subscript

A	$CuSO_4$
B	H_2SO_4
0	reference value
1	Cu^{2+} ion
2	H^+ ion
I	He–Ne laser
II	Ar laser

References

1. C. Wagner, *J. Electrochem. Soc.*, **95**, 161 (1949).
2. N. Ibl and R. H. Muller, *J. Electrochem. Soc.*, **105**, 346 (1958).
3. C. R. Wilke, M. Eisenberg, and C. W. Tobias, *J. Electrochem. Soc.*, **100**, 513 (1953).
4. C. Wagner, *J. Electrochem. Soc.*, **98**, 116 (1951).
5. J. R. Selman and J. Newman, *J. Electrochem. Soc.*, **118**, 1070 (1971).
6. Y. Fukunaka, K. Denpo, M. Iwata, K. Maruoka, and Y. Kondo, *J. Electrochem. Soc.*, **130**, 2492 (1983).
7. K. Denpo, T. Okumura, Y. Fukunaka, and Y. Kondo, *J. Electrochem. Soc.*, **132**, 1145 (1985).
8. K. Asada, F. Hine, S. Yoshizawa, and S. Okada, *J. Electrochem. Soc.*, **107**, 242 (1960).

9. J. R. Lloyd, E. M. Sparrow, and E. R. G. Eckert, *J. Electrochem. Soc.*, **119**, 702 (1972).
10. Y. Awakura, A. Ebata, and Y. Kondo, *J. Electrochem. Soc.*, **126**, 23 (1979).
11. Y. Fukunaka, Y. Nakamura, and Y. Konishi, *J. Electrochem. Soc.*, **145**, 3814 (1998).
12. Y. Konishi, Y. Tanaka, Y. Kondo, and Y. Fukunaka, *Electrochim. Acta*, **46**, 681 (2000).
13. Y. Konishi, Y. Nakamura, Y. Fukunaka, K. Tsukada, and K. Hanasaki, *Electrochim. Acta*, **48**, 2615 (2003).
14. J. R. Selman and C. W. Tobias, *J. Electroanal. Chem.*, **65**, 67 (1975).
15. J. Newman, *J. Electrochem. Soc.*, **113**, 1235 (1966).
16. V. Marathe and J. Newman, *J. Electrochem. Soc.*, **116**, 1704 (1969).
17. W. H. Smyrl and J. Newman, *J. Electrochem. Soc.*, **118**, 1079 (1971).
18. R. V. Homsy and J. Newman, *J. Electrochem. Soc.*, **121**, 521 (1974).
19. C. M. Mohr, Jr. and J. Newman, *J. Electrochem. Soc.*, **123**, 1687 (1976).
20. W. R. Parrish and J. Newman, *J. Electrochem. Soc.*, **116**, 169 (1969).
21. W. R. Parrish and J. Newman, *J. Electrochem. Soc.*, **117**, 43 (1970).
22. R. Alkire and A. A. Mirarefi, *J. Electrochem. Soc.*, **120**, 1507 (1973).
23. R. Alkire and A. A. Mirarefi, *J. Electrochem. Soc.*, **124**, 1043 (1977).
24. R. Alkire and A. A. Mirarefi, *J. Electrochem. Soc.*, **124**, 1214 (1977).
25. M. Georgiadou, *J. Electrochem. Soc.*, **144**, 2732 (1997).
26. F. H. Bark and F. Alavyoon, *J. Fluid Mech.*, **290**, 1 (1995).
27. V. M. Volgin, O. V. Volgina, D. A. Bograchev, and A. D. Davydov, *J. Electroanal. Chem.*, **546**, 15 (2003).
28. S. Kawai, K. Nishikawa, Y. Fukunaka, and S. Kida, *Electrochim. Acta*, **53**, 257 (2007).
29. S. Kawai, Y. Fukunaka, and S. Kida, *J. Electrochem. Soc.*, **155**, F75 (2008).
30. F. R. McLarnon, R. H. Muller, and C. W. Tobias, *J. Electrochem. Soc.*, **122**, 59 (1975).
31. F. R. McLarnon, R. H. Muller, and C. W. Tobias, *J. Opt. Soc. Am.*, **65**, 1011 (1975).